



Journal of Applied and Computational Mechanics



Research Paper

Nonlinear Multiscale Modelling and Design using Gaussian Processes

Sumudu Herath¹, Udith Haputhanthri²

¹ Department of Civil Engineering, University of Moratuwa, Sri Lanka, Email: sumuduh@uom.lk

² Department of Electronic and Telecommunication Engineering, University of Moratuwa, Sri Lanka, Email: 170208k@uom.lk

Received December 20 2020; Revised March 05 2021; Accepted for publication March 10 2021.

Corresponding author: S. Herath (sumuduh@uom.lk)

© 2021 Published by Shahid Chamran University of Ahvaz

Abstract. A method for nonlinear material modeling and design using statistical learning is proposed to assist in the mechanical analysis of structural materials. Conventional computational homogenization schemes are proven to underperform in analyzing the complex nonlinear behavior of such microstructures with finite deformations. Also, the higher computational cost of the existing homogenization schemes inspires the inception of a data-driven multiscale computational homogenization scheme. In this paper, a statistical nonlinear homogenization scheme is discussed to mitigate these issues using the Gaussian Process Regression technique. A data-driven model is trained for different strain states of microscale unit cells. In the macroscale, nonlinear response of the macroscopic structure is analyzed, for which the stresses and material responses are predicted by the trained surrogate model.

Keywords: Gaussian processes, multiscale modelling, material modelling, statistical learning, data-driven continuum mechanics.

1. Introduction

Nonlinear structural materials have gained increasing popularity over the past years due to their tailorable material properties and finite strain deformability. These tailorable properties include stretch forming and deep drawing formability that exhibits excellent stretchability and drapeability properties of such materials [1]–[3]. Since the inception of additive manufacturing in various industrial applications, a multitude of 3D printable materials paved their way into creating structural assembly components. These industrial applications include, but certainly not limited to: aerospace, biomedical, civil engineering, defense, marine and medical industries [4], [5]. For instance, the rapid boost in additive manufacturing technologies discovered ways of producing highly-flexible textiles using digital interlacing and digital interlooping of fibers. These textiles possess highly nonlinear stress-strain relationships due to their inherent finite strain deformability. Besides, digital interlooping unfolds ways to reinforce the traditional knitting stitches by inserting high-strength fibers in course and wale directions [1]. Reinforced biaxial weft-knitted textile composite is one such invention. Digital interlacing, on the other hand, uses warp and fill fibers to manufacture woven textiles by automating the weaving process of a traditional loom apparatus [6], [7].

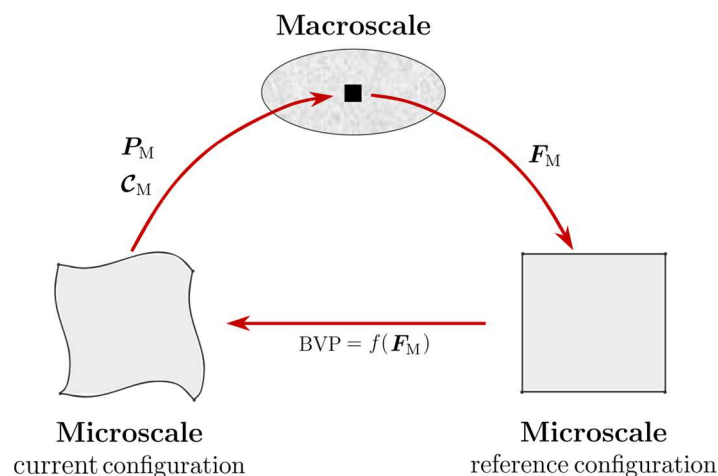


Fig. 1: Conventional computational homogenization scheme for a two-scale problem



Estimating constitutive behavior of nonlinear elastic materials is one of the challenging tasks in understanding different structural materials. In a big picture, these elastic materials can be Cauchy elastic, hypoelastic or hyperelastic [8], [9]. These materials exhibit highly nonlinear constitutive laws where traditional experimental setups or numerical solvers find it nearly impossible to accurately predict the material relationships, especially at higher strains. Besides, the geometric complexity and constituent uncertainty of finite deformable structures restrict the conventional analysis tools on accurate material property estimation and modeling.

This restriction is evident as the existing numerical solvers are not sophisticated in terms of finite deformations, parametric uncertainties, geometric sensitivities and material phase interactions [10], [11]. This paper focuses on a class of structural materials where a repetitive unit cell, or a Representative Volume Element (RVE) characterize the complete structural geometry.

Multiscale modeling is the tool of choice in analyzing such structures with one or more RVEs. Multiscale methods, in general, aim to predict the macroscopic behavior of engineering materials through a systematic and consistent modeling of the fundamental mechanics and physics of underlying microstructures [12]–[15] (see Fig. 1). These microstructures can be of different scales and capable of capturing various mechanical responses such as material nonlinearities [2], [3], [5]; cracks in 3D space and semi-concurrent FE-FE coupling [16]; fracture modelling [17]. Diverse applications of multiscale techniques have been identified in numerous scientific research domains such as; modelling of defect kinetics in irradiated iron [3], [18], heterogeneous catalysis [2], [19], modelling of plastic flow localization in irradiated materials [3], [20], textile modelling [2], [3], [7], [19], [20], [21] crystalline lattice defect detection modelling [4] [20] and heterogeneous composite modelling [10]. A proper understanding of the microscale behavior, evolution, and mechanical response of materials is critical in modeling such microstructures [22]. In general, these microstructures have a multitude of variables that governs the homogenized response in the macroscale. Such variables can be highly uncertain but also have a significant influence on the homogenized response [12]. For instance, particles embedded in a matrix, as shown in Fig. 2, can have an infinite number of realizations for a given particle volume fraction. But depending on the particle distribution in the matrix, macroscale quantities can vary significantly to one another. Therefore, it is of paramount importance to study such variations in the macroscale quantities for perturbations in the microstructural quantities. However, well-established and fully analytically tractable conventional multiscale modeling techniques inherently comes with the disadvantages highlighted above. Specifically, multiscale techniques are extremely expensive when the problem domain is larger [5]. Also, those methods are insensitive to parametric uncertainties of the embedded constituents and therefore lack the flexibility to study the sensitivities at the minimum cost [10]. This paper proposes a framework, illustrated in Fig. 3, with the aid of statistical learning to circumvent the aforementioned problems of conventional multiscale techniques in the context of structures with one repetitive RVE.

Statistical learning is a new trending field these days and is seen as a subset of artificial intelligence (AI). Statistical learning uses several statistical algorithms to make computers think in a certain way without being explicitly programmed [23], [24]. These algorithms receive an input value (or vector) and predict an output (s) for this through the use of statistical methods. The strong versatility of statistical learning outclassed traditional statistical modeling techniques, which paved the way for it to be used in diverse fields such as cyber-security, banking, finance, military, healthcare, robotics, automotive, social media and mass transportation. Trend identification, handling multi-dimensional and multi-variety data, automation of algorithmic computations are few of the many merits of machine learning that attract computational structural mechanics communities [10]. Notwithstanding, the time taken for model training, the accuracy of predictions, compatibility within a finite element environment are challenges that need special attention in the process of integrating machine learning methods in a finite element solver [25]. These challenges can be systematically overcome by a thorough understanding of the strengths and weaknesses of various machine learning techniques: neural networks, kernel methods, sparse kernel machines, graph models [24]. Although, neural networks have been the tool of choice in various cutting edge applications [25], [26], [27] and many machine learning communities, we qualitatively evaluate the use of deep learning in our applications.

Therefore, a research gap is identified to propose a unified framework to predict the nonlinear material response of structures with one RVE. This framework is developed with the aid of statistical learning integrated into conventional multiscale modeling. This paper aims to timely bridge the recent additive manufacturing advancements with the proposed unified analysis tools.

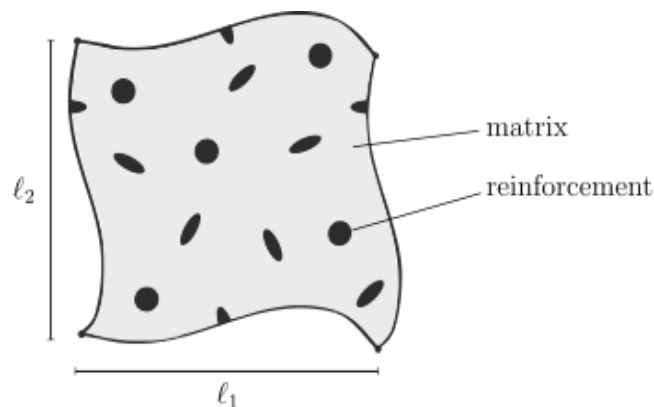


Fig. 2: Generalised RVE of a composite material with microstructural particles (reinforcement)

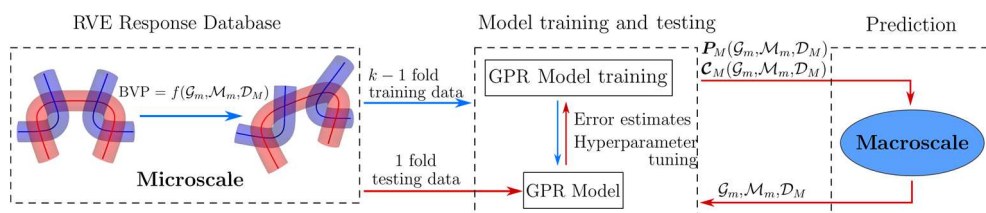


Fig. 3: Data-driven computational homogenization and material designing framework using Gaussian Process Regression machine learning



This section introduced the reader to the big picture of this research work by highlighting the background, research gap and the motivation behind the work. Section two discusses on Gaussian process statistical learning technique and Section three integrates the conventional multiscale modeling with Gaussian processes. Section four presents a neat example using knitted membranes to validate the proposed framework. Section five concludes the paper by outlining the key contributions and results.

2. Gaussian process regression (GPR)

2.1 Gaussian processes

Gaussian process is a method of statistical inference based on the Bayesian statistical learning technique. In this section, we present the key formulations of a Gaussian process and readers are kindly invited to refer to Rasmussen et al. [28] for further details. We write a zero-mean prior Gaussian process of a database with \mathbf{z} being an input variable vector of size $1 \times d$, as,

$$F(\mathbf{z}) \sim GP(\mathbf{0}, k(\mathbf{z}, \mathbf{z}')) \quad (1)$$

where d is the number of features in \mathbf{z} . Moreover, the covariance function $k(\mathbf{z}, \mathbf{z}')$ is chosen to be a squared exponential function given by,

$$k(\mathbf{z}, \mathbf{z}') = \sigma_f^2 \exp\left(-\frac{(\mathbf{z} - \mathbf{z}')^T (\mathbf{z} - \mathbf{z}')}{2\ell^2}\right) \quad (2)$$

where σ_f and ℓ are the scaling and lengthscale hyperparameters, respectively. For convenience, we define $\boldsymbol{\theta} = (\ell, \sigma_f)$ as the vector of hyperparameters.

Now we consider a database comprising of training and testing datasets. Each data point is given by an input vector \mathbf{z}_i and a target (observation) y_i where $i = 1, 2, \dots, N$. Training data points are denoted as (Z, y) and testing data points are denoted by (Z_*, y_*) . Moreover, entries of the covariance matrix K are given by $K_{ij} = k(\mathbf{z}_i, \mathbf{z}_j)$. To this end, the joint distribution of training and test outputs are written as,

$$\begin{bmatrix} y \\ y_* \end{bmatrix} \sim N\left(0, \begin{bmatrix} K(Z, Z) & K(Z, Z_*) \\ K(Z_*, Z) & K(Z_*, Z_*) \end{bmatrix}\right) \quad (3)$$

Predictions based on the conditioning of the joint Gaussian prior distribution on the observations and test inputs follows a Gaussian distribution as,

$$y_* | Z_*, Z, y \sim N(K(Z_*, Z)K(Z, Z)^{-1}y, K(Z_*, Z_*) - K(Z_*, Z)K(Z, Z)^{-1}K(Z, Z_*)) \quad (4)$$

Hence the best estimate for y_* is the mean of the above distribution given by,

$$\bar{y}_* = K(Z_*, Z)K(Z, Z)^{-1}y \quad (5)$$

And the uncertainty of the estimate is given by the variance of the Gaussian distribution as,

$$\text{var}(y_*) = K(Z_*, Z_*) - K(Z_*, Z)K(Z, Z)^{-1}K(Z, Z_*) \quad (6)$$

2.2 Hyperparameter estimation

Now it is important to establish a systematic approach to find the optimum hyperparameters that give the best fit to the data in hand. To achieve this first we establish the relationships between the posterior $P(\boldsymbol{\theta} | y, Z)$, likelihood $P(y | Z, \boldsymbol{\theta})$, prior $P(\boldsymbol{\theta})$ and marginal likelihood $P(y | Z)$ as,

$$P(\boldsymbol{\theta} | y, Z) = \frac{P(y | Z, \boldsymbol{\theta})P(\boldsymbol{\theta})}{P(y | Z)} \quad (7)$$

To this end, we expand the marginal likelihood using eq. (7) as,

$$P(y | Z) = \int P(y | Z, \boldsymbol{\theta})P(\boldsymbol{\theta})d\boldsymbol{\theta} \quad (8)$$

Marginal likelihood in eq. (8) can be further simplified by taking the logarithm to arrive at the log marginal likelihood,

$$\log P(y | Z) = -\frac{1}{2}y^T K^{-1}y - \frac{1}{2}\log|K| - \frac{N}{2}\log 2\pi$$

where $|K|$ is the determinant of the matrix K and last term is a constant with N being the database size [28].

Determination of the hyperparameters $\boldsymbol{\theta}$ departs from maximising the log marginal likelihood, with respect to hyperparameters $\boldsymbol{\theta}$. We use scikit-learn Python library [29] to find the maximum log marginal likelihood (MLML) and corresponding optimal hyperparameters. MLML requires the partial derivatives of the log marginal likelihood with respect to hyperparameters. This is written as,

$$\frac{\partial}{\partial \theta_j} \log P(y | Z) = \frac{1}{2} \text{Tr} \left((\Phi \Phi^T - K^{-1}) \frac{\partial K}{\partial \theta_j} \right)$$

where $\Phi = K^{-1}y$ and $\text{Tr}()$ is the standard trace operator of a square matrix.

2.3 Quantitative error metrics

GPR model is iteratively evaluated for error estimates under the cross-validation technique by using $k - 1$ folds for model training and the remaining one for model testing (see Fig. 3). In this paper, we have used $k = 5$ which is proven to be a good compromise between accuracy and efficiency [30]. Moreover, we use two error metrics, namely correlation of determination R^2 and mean squared error (MSE) to assess the errors of the predicted strain energy density and stress components. These errors are given by,

$$R^2(y, \hat{y}) = 1 - \frac{\sum_{i=1}^N (y_i - \hat{y}_i)^2}{\sum_{i=1}^N (y_i - \bar{y})^2} \quad (9)$$



$$\text{MSE}(y, \hat{y}) = \frac{1}{N} \sum_{i=1}^N (y_i - \hat{y}_i)^2 \quad (10)$$

where y_i , \hat{y} and \bar{y} stand for target output, predicted output and mean of the target outputs, respectively. When evaluating the MSE of the predicted stress tensor, we take the square-root of the squared sum of the MSE of each stress component, given by,

$$\text{MSE}(S, \hat{S}) = \sqrt{\sum_{i=1}^2 \sum_{j=1}^2 \text{MSE}^2(S_{ij}, \hat{S}_{ij})} \quad (11)$$

2.4 Differentiation of Gaussian processes

Many applications require the partial derivatives of predictions with respect to the input variables. In the computational mechanics context of a hyperelastic material, predicted strain energy (ψ) needs to be differentiated with respect to the Green-Lagrange strain tensor (\mathbf{E}) components to arrive at the second Piola-Kirchhoff stress tensor (\mathbf{S}) components. Moreover, because differentiation is a linear operation, a derivative of a Gaussian process remains a Gaussian process [28], [31].

Consider a single new data point as \mathbf{z}_* . Thus $K(\mathbf{Z}_*, \mathbf{Z})$ matrix has one row and d number of columns. The aim is to find the partial derivatives with respect to this new test point \mathbf{z}_* .

$$\frac{\partial \bar{y}_*}{\partial \mathbf{z}_*} = [\hat{\mathbf{Z}}_*^T (k(\mathbf{z}_*, \mathbf{Z})^T \odot K(\mathbf{Z}, \mathbf{Z})^{-1} \mathbf{y})] \quad (12)$$

where $\hat{\mathbf{Z}}_*$ is given by $[\mathbf{z}_* - \mathbf{z}_1, \mathbf{z}_* - \mathbf{z}_2, \dots, \mathbf{z}_* - \mathbf{z}_n]^T / \ell^2$ and \odot denotes an element-wise product, also known as Hadamard or Schur product. That is, for two vectors of the same size (say $N \times 1$), $(\mathbf{a} \odot \mathbf{b})_i = a_i b_i$ for $i = 1, 2, \dots, N$, where summation convention is not implied over i .

Next, second-order partial derivatives are obtained following a similar manner. In a computational mechanics context, these second derivatives are analogous to the fourth-order material tangent tensor. That is, $\mathbf{C} = \partial^2 \psi / \partial \mathbf{E} \partial \mathbf{E}$. In addition, $\boldsymbol{\alpha} = K(\mathbf{Z}, \mathbf{Z})^{-1} \mathbf{y}$ has been used henceforth to simplify the expressions as it is not a \mathbf{z}_* dependent.

Now we differentiate eq. (12) to derive the second partial derivative of the posterior mean as,

$$\frac{\partial^2 \bar{y}_*}{\partial^2 \mathbf{z}_*} = - \sum_{i=1}^n \left(\mathbf{I} - (\mathbf{z}_* - \mathbf{z}_i) \otimes (\mathbf{z}_* - \mathbf{z}_i) \right) k(\mathbf{z}_*, \mathbf{z}_i) \boldsymbol{\alpha}_i / \ell^4.$$

Formulations presented in this section are used in the *Model training and testing* stage of the proposed data-driven nonlinear multiscale modeling framework presented in F.

3. Data-driven nonlinear multiscale modeling

3.1 Review on Multiscale modeling

Different classifications have been suggested to categorize multiscale methods. One classification divides the manifold multiscale methods as concurrent, hierarchical and hybrid methods [12], [13]. In this paper, and also the method of choice in the mechanics community, we focus on the hierarchical multiscale methods. In the hierarchical methods, the scales are coupled in a hierarchical manner, which implies that different scales are considered and linked in the same part of a domain. The hierarchical link is usually established through volume averaging of field variables, and different scales are solved in parallel to arrive at the global equilibriums in all scales. Moreover, this paper focuses only on twoscale problems where two distinct scales are named as macroscale and microscale (or finescale). On a big picture, the hierarchical link for general twoscale problems follows the traditional loop strategy as depicted in Fig. 1. It is important to understand the two main scale transitions as macro-to-micro and micro-to-macro that complete the loop in Fig. 1.

Deformation gradient \mathbf{F}_M is the macroscale quantity that departs from the macroscale to formulate a boundary value problem at the microscale. Next, resulting forces \mathbf{P}_M and force tangents \mathbf{C}_M are extracted from the current configuration to solve the boundary value problem at the macroscale. The most commonly used scale transition to establish the macro-to-micro coupling is the kinematical averaging relation. It requires the volume averaged microscale deformation gradient tensor \mathbf{F}_m , to be equal to the macroscale deformation gradient tensor \mathbf{F}_M , which takes the form,

$$\mathbf{F}_M = \frac{1}{V_0} \int_{V_0} \mathbf{F}_m dV \quad (13)$$

where V_0 refers to the reference volume of the microscale RVE. Based on the Hill-Mandel energy conservation relation [12], the macroscale first Piola-Kirchhoff stress tensor can simply be identified as the volume average of the microscale first Piola-Kirchhoff stress tensor, as the following.

$$\mathbf{P}_M = \frac{1}{V_0} \int_{V_0} \mathbf{P}_m dV \quad (14)$$

In linear multiscale modeling, it is not necessary to compute the material tangents at every integration point, as the linearity priori assumes the material tangent to be constant at any material point in the macroscale. However, in nonlinear multiscale modeling it is important to extract the force tangents at every strain level. Extraction of the material tangent matrices has been approached using a forward difference method by Nadler et al. [7]. Moreover, schemes that employ a direct condensation of the constrained degrees of freedoms are considered to extract the (integration) point-wise material tangent matrices [12], [13]. In our method, we simply use the second derivative of the trained Gaussian process model to find these force tangents. Therefore, our method is efficient in comparison to point-wise iterative schemes mentioned above.

Now we discuss the three main ingredients of the proposed framework shown in Fig. 3 as these three ingredients forms the basis of the proposed unified framework.



3.2 RVE response database construction

Development of a complete space-filling response database is pivotal in machine learning. This is achieved by designing experiments to simulate microscale RVEs constrained by predefined BVPs. These BVPs, as shown in Fig. 3, have three main ingredients, namely Geometric, Material and Deformation. These ingredients are chosen from the standpoints of both mechanical analysis (Deformation) and material system designing (Geometric and Material) to widen the scope of using machine learning in this domain. It is straightforward to use more ingredients in constructing the response databases, however, we argue that those ingredients will also fall into the three broad categories defined above.

3.2.1 Geometric properties

Geometric properties include RVE spatial dimensions, yarn cross-section properties (for fiber-based RVEs), initial curvatures (or angles), waviness parameters of sinusoidal RVEs etc. Care should be taken when there are intrinsic relationships between two geometric properties. Geometric properties govern the *material design* aspects of the proposed framework in Fig. 3.

3.2.2 Material properties

Material properties of a RVE refer to the Young's moduli and Poisson's ratios of a general heterogeneous linear material model. Material nonlinearities can also be included in a systematic manner. Material properties also govern the *material design* aspects of the proposed framework in Fig. 3.

3.2.3 Deformation states

Deformation states provide the basis of *multiscale modeling*. Usually, deformation states are taken to be any strain tensor (small strain, Euler-Almansi, logarithmic, Green-Lagrange), deformation gradient or a combination of displacements and rotations. In this paper, we use the deformation gradient F_M to apply boundary constraints. These deformation states are applied using Periodic Boundary Conditions (PBCs) at the boundaries of the RVE. Hence, various combinations of boundary conditions in the macroscale can be easily accommodated as we have embedded respective deformation gradients at the microscale simulations.

To provide the readers with a better picture of the three different design variables, we include all three design categories (G_m , M_m and D_M) in the feature space of a response database. For a general 2D RVE given in Fig. 2 we write the domain of all three design variables (see Fig. 3) bounded by predefined limits as follows. Here, we consider the plane-stress state of the RVE shown above. Therefore, in D_M we have only the in-plane strain components to characterize the deformation states. Moreover, subscripts *mat* and *r* refer to reinforcement material particles and the embedded resin, respectively.

$$G_m = \begin{cases} G_m^1 = \ell_1 & \ell_1 \in [\ell_1^{\min}, \ell_1^{\max}] \\ G_m^2 = \ell_2 & \ell_2 \in [\ell_2^{\min}, \ell_2^{\max}] \end{cases} \quad (15)$$

$$M_m = \begin{cases} M_m^1 = E_{\text{mat}} & E_{\text{mat}} \in [E_{\text{mat}}^{\min}, E_{\text{mat}}^{\max}] \\ M_m^2 = \nu_{\text{mat}} & \nu_{\text{mat}} \in [\nu_{\text{mat}}^{\min}, \nu_{\text{mat}}^{\max}] \\ M_m^3 = E_r & E_r \in [E_r^{\min}, E_r^{\max}] \\ M_m^4 = \nu_r & \nu_r \in [\nu_r^{\min}, \nu_r^{\max}] \\ M_m^5 = N_p & N_p \in [N_p^{\min}, N_p^{\max}] \end{cases} \quad (16)$$

$$D_M = \begin{cases} D_M^1 = E_{11} & E_{11} \in [E_{11}^{\min}, E_{11}^{\max}] \\ D_M^2 = E_{22} & E_{22} \in [E_{22}^{\min}, E_{22}^{\max}] \\ D_M^3 = E_{12} & E_{12} \in [E_{12}^{\min}, E_{12}^{\max}] \end{cases} \quad (17)$$

where N_p is the number of reinforcement particles in the RVE in Fig. 2.

3.3 GPR model training and testing

We start by randomly shuffling the data points in the response database. Next, the response database is split into equal (approximately) k folds for k fold cross-validation. Empirically proven values for k take values $k = 5, 10$ [24], [30]. The special case of $k = 1$ is known as Leave One Out Cross-Validation (LOOCV). As shown in Fig. 3, $k - 1$ fold data from the randomly shuffled response database is used to train a GPR model and the remaining fold, in turn, is used to test the trained model. In simple terms, the process is repeated k times until every fold becomes a test fold. In this paper, we use $k = 5$. During this process, it is essential to establish performance indicators to quantitatively and qualitatively assess cross-validation.

Overfitting and underfitting are two of the most prevalent machine learning challenges. There are several ways to circumvent these two challenges in relation to Gaussian processes. Overfitting occurs in analyses that regress too closely or exactly to a particular set of data, and may therefore, fail to fit new data or predict future observations reliably. A simple example would be to fit three (non-coincident) collinear points using a polynomial of degree more than one. A quadratic or any higher degree polynomial can exactly represent the given three points but the data, in reality, could be following a simple linear model. Therefore, when a model is overfitted, we observe very low MSE and R^2 close to 1 for the training dataset but not for the testing dataset [30], [32]. In contrast, underfitting, as the name implies, refers to a model that does not fit well even for the training data. Intuitively, underfitting occurs when the model cannot trace the underlying trend of the training data. Imagine using a linear model to capture the trend of a dataset that in reality follows a high-amplitude sinusoid. Underfitting always leads to a comparatively higher MSE and near-zero R^2 values for the training dataset.

Hyperparameter tuning keeps track for any occurrences of overfitting or underfitting [29]. From our experience, GPR models usually do overfit but not underfit. This happens mainly due to the use of infinitely smooth squared exponential covariance functions. Overfitting is triggered when hyperparameters reach their predefined lower bounds or when the hyperparameter bounds are too wide. In addition to very low training errors and high testing errors, overfitting is revealed when optimized hyperparameters and MLML significantly differ in each fold of k fold cross-validations. When this happens, the hyperparameter setting is revised so that overfitting is avoided in the final GPR model. Once overfitting is flagged in the scikit-learn algorithm [29], hyperparameter tuning is conducted by systematically varying the hyperparameter bounds (*length_scale_bounds*) and simultaneously monitoring the convergence of the MLML for each k fold. In some cases, overfitting was avoided by a combination of the aforementioned hyperparameter bound variation and using different initial lengthscale (*length_scale*) values.



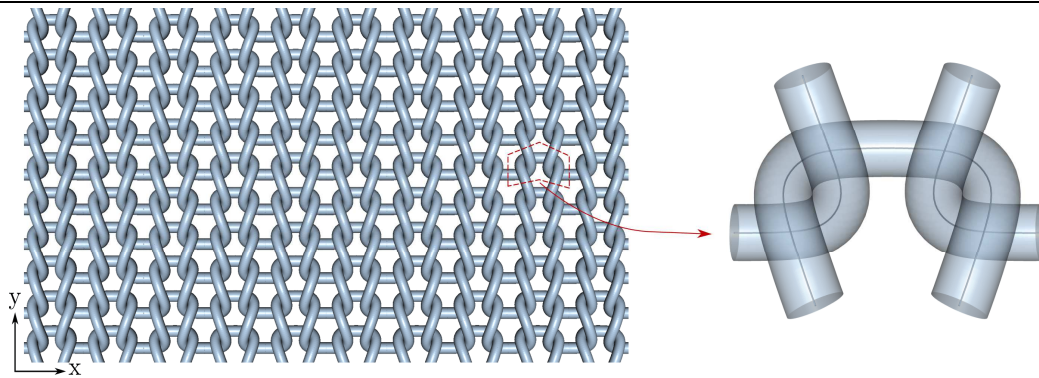


Fig. 4: Selection of a multiscale analysis-suitable RVE of the weft-knitted textile

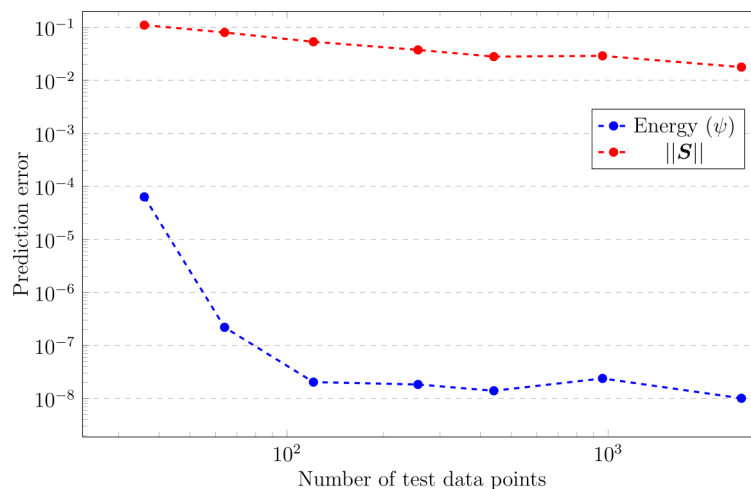


Fig. 5: Errors of the predicted strain energy density and the norm of the vectorized second Piola-Kirchhoff stress tensor components

3.4 Prediction

Lastly, the trained GPR model is used to make predictions based on new data points departing from the macroscale problem. At the reference (stress-free) configuration, all three strain components (zero in magnitude) will arrive at the trained GPR model to predict the internal strain energy density, first Piola-Kirchhoff stress tensor and material constitutive tensor. Likewise, at every load step and equilibrium iteration, the enlisted strain components at integration points will communicate with the GPR model to make predictions. This step is illustrated in Fig. 3 as the third key step in the proposed data-driven homogenization technique.

4. Results and Discussion

4.1 Multiscale modeling of knitted membranes

The motivation to use knitted membranes to illustrate the data-driven nonlinear material modeling is twofold. First, knitted materials have gained an increasing levels of interests among researchers due to their efficient load transferring mechanisms [1]–[3], [33]. Secondly, the complex geometric and nonlinear mechanical response of knitted membranes set a good benchmark to test the proposed framework, than resorting to simpler problems.

Knitting is the process of making textiles by interlooping a thread (yarn) where, in contrast, weaving involves interlacing of two or more yarns. On a broad picture, we identify two main types of knitted textiles: warp-knitting and weft-knitting. While weft-knitted textiles are easily handmade and commonly used, warp-knitted textiles are popular products of knitting machines. In this paper, we focus only on weft-knitted membranes. As common to any multiscale strategy, the first task is to identify an element to represent the macroscale continuum (see Fig. 4). This RVE shown in Fig. 4 is geometrically modeled using cubic B-splines. The tedious geometric equations of a weft-knitted textile RVE can be found in Vassiliadis et al. [33], [34] and Weeger et al. [3]. Also, the Young's modulus of the yarn was taken as 800 MPa. This fibrous weft-knitted RVE is modeled in an in-house finite element environment using finite deformable rods with non-frictional contacts.

4.2 Microscale model verification

As the first task in constructing response database for statistical learning, we must ensure that the numerical model in hand is accurate. Therefore, we conduct strip biaxial and shear tests on weft-knitted RVEs, and compare them with the independent results in literature. Result comparison is presented in Fig. 5, and we conclude our microscale RVE simulations approximate the experimental results very well, and follow a better trend than that of the numerical results from Weeger et al. [3] and Dinh et al. [s2]. It is evident that the homogenized responses of strip biaxial tests are nonlinear and RVEs are stiffened (increasing gradients) at higher strains. Moreover, the shear response is observed to be nearly linear. Thus, shear stiffnesses at each strain level can be considered constant and comparatively lower. We can safely assume there are no axial-shear coupling effects due to yarn alignments depicted in Fig. 5. Therefore, we use a constant shear modulus in macroscale simulations to relate shear strains to shear stresses.



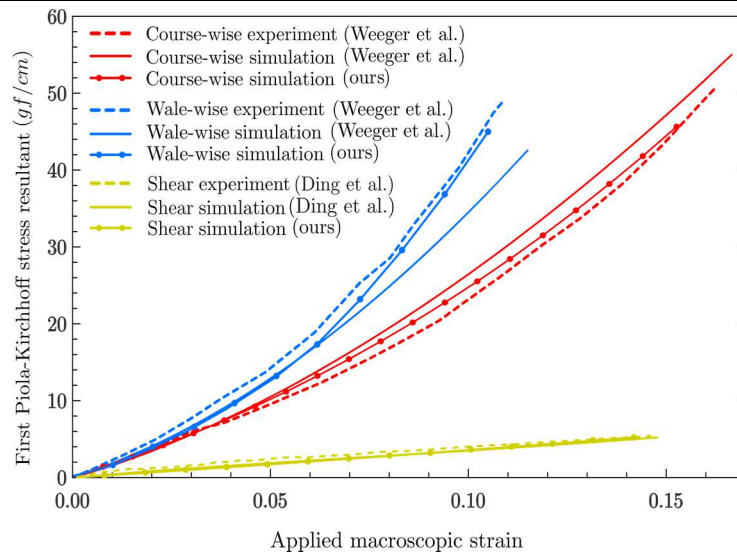


Fig. 6: Comparison of simulation results for course-wise and wale-wise strip biaxial tension and pure shear test against the experimental results from literature

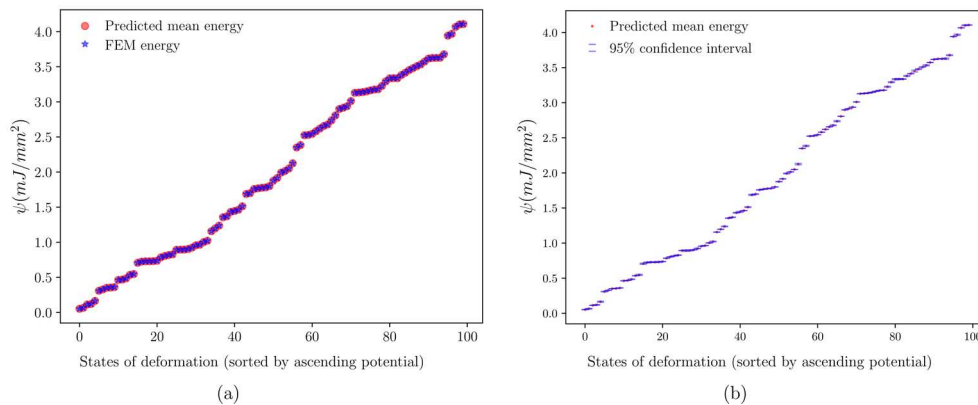


Fig. 7: (a) Strain energy prediction for unseen data points sorted by ascending potentials (b) 95% confidence interval of the predicted mean energy

4.3 Data-driven multiscale modeling of nonlinear knitted membranes

We construct the response database using three in-plane strain components as inputs and volume averaged energy as the output. This is succinctly written as $(\mathbf{z}, y) = (E_{11}, E_{12}, E_{22}, \psi)$. Moreover, the Sobol sequence quasi-random sampling technique is used to sample the points in the database. Sampling bounds are chosen as $[-0.05, 0.15]$ for axial strains and $[0, 0.15]$ for shear strains.

It is of paramount importance to maintain algorithmic efficiency when training GPR models. In Fig. 7, we present the variability of GPR model testing errors for energy and stress predictions. Equation (10) is used to compute the mean squared errors of energy predictions. Errors in stress predictions are comparatively higher than the energy predictions. This observation is natural in data-driven analyses because the derivative of a data-fitted model is considered as an approximation of an approximation [24], [28]. Additionally, it is observed that error in stress components is comparatively higher closer to the domain boundary (see Fig. 8) which again is due to the lesser accurate derivative approximations at the boundary. However, the minimum MSE was recorded as 1.98% which is better in comparison to the similar work by Bessa et al. [35]. And this is also due to the fact that MSE is not a normalized measure of error, hence the error convergence depends on the magnitude of the quantity being measured. Normalized minimum MSE of stress was recorded as 1.68×10^{-5} , where the normalization quantity is defined as $\text{MSE}(S, 0)$. Considering the error convergence and algorithmic efficiency, we use a response database with 13005 data points (thus 2601 test data per each fold k) in subsequent analyses.

A small but complete subset of the full database is extracted to train a GPR model. As shown in Fig. 6, we use 100 new data points from the full database to test the accuracy of the trained GPR model. Fig. 6 also presents the corresponding 95% confidence interval of the predicted energy of the new data points. For this particular database, training and testing errors were recorded as 1.72×10^{-11} and 0.82×10^{-5} . Optimized hyperparameters values $\Theta = (\sigma_f, \ell)$ and maximum log marginal likelihood values were recorded as 1.25321, 0.009042 and 9594.9821, respectively. Time taken for model training was recorded as 31 minutes and 28 seconds on an Intel Core i5-4590 CPU 3.30GHz x 4 processor.

Accuracy test on predicted energy has to be followed by an accuracy test on the stress components. Using MSE for stress components, we evaluate the degree of accuracy of the predicted stresses to that of observed stresses in the database. Fig. 8 provides two principal stress component comparisons, thus setting shear strains to zero. For visualization purpose, one strain component is held constant while the other is increased from 0.0 to 0.16. We can observe nearly exact stress predictions from the trained GPR model. Moreover, we notice slight deviations close to the bounds of strain components which is treated by refining the data points close to these bounds. These errors close to feature space bounds are common in statistical learning applications due to the inability of extrapolation beyond the domain boundaries.



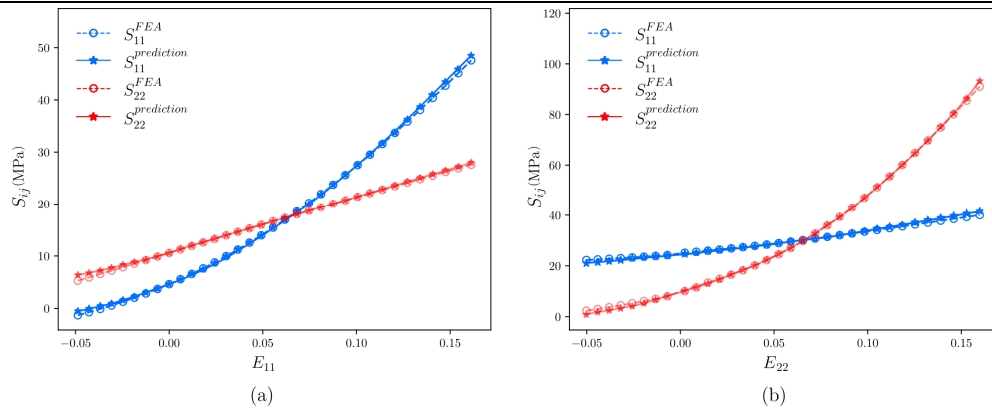


Fig. 8: Prediction and comparison of the second Piola-Kirchhoff stress resultants. (a) S_{11} , S_{22} for $E_{11} = [0.%, 22%]$ and $E_{22} = 8%$. (b) S_{11} , S_{22} for $E_{22} = [0.%, 22%]$ and $E_{11} = 10%$.

Merits of the proposed multiscale modelling and design framework were discussed in detail in Sections 2 and 3, respectively on GPR technique and analysis and design aspects of knitted membranes. However, some limitations of this method are identified which are mainly application-based. Implementing this framework directly on plastic material models will lead to less accurate results as smooth kernel functions might find it difficult to approximate non-smooth material models. Also, in comparison to deep learning algorithms, GPR algorithms are not well optimized for handling very large databases, therefore will lead to computationally expensive models in the event of GPs models with very large databases.

This section illustrated the multiscale modeling of weft-knitted membranes using the proposed framework in Fig. 3. Detailed discussions on response database construction, GPR model training and testing are provided to explain the step by step process in the proposed data-driven multiscale modeling technique. In addition, error convergence and result comparisons are also provided to showcase the accuracy of the implementations.

5. Conclusion

A generalized statistical learning method for multiscale modeling of nonlinear materials is proposed to address the challenges posed by conventional homogenization schemes. Large deformations prevalent in structural materials are accurately captured by the proposed method using weft-knitted membranes as an example. Incorporating GPR in a multiscale modeling environment circumvents the need for element-wise microscale simulations, thus yields significant computational savings. Also, the inclusion of design parameters in the frameworks was shown to open avenues for efficient nonlinear material system designs.

Author Contributions

S. Herath established the theoretical background; initiated the project; developed the mathematical modeling and examined the theory validation, and derived the unified numerical framework; U. Haputhanthri conducted the numerical experiments, constructed databases and analyzed the simulation results. The manuscript was written through the contribution of all authors. All authors discussed the results, reviewed, and approved the final version of the manuscript.

Acknowledgments

Discussions with Prof. Mark Girolami and Dr. Fehmi Cirak from the Computational Mechanics Laboratory at the University of Cambridge and Dr. Chinthaka Mallikarachchi at University of Moratuwa are acknowledged.

Conflict of Interest

The authors declared no potential conflicts of interest with respect to the research, authorship, and publication of this article.

Funding

The authors received no financial support for the research, authorship, and publication of this article.

Nomenclature

$(\cdot)_m$	Quantity in macroscale	S	Second Piola-Kirchhoff stress tensor
$(\cdot)_M$	Quantity in Macroscale	V_0	The reference volume of the microscale RVE
C	Fourth-order material tangent tensor	y	Target (observation)
D_M	Deformation design variable	Z	Gram matrix
d	The number of features in z	z	Generalized input variable
E	The Green-Lagrange strain tensor	θ	Vector of hyperparameters.
F	Deformation gradient tensor	σ_f	Scaling hyperparameter
G_m	Geometric design variable	Φ	$\Phi = K^{-1}y$
K	Covariance matrix	ψ	Strain energy




ℓ	Lengthscale hyperparameter	$a \odot b$	Vector element-wise product (Hadamard product)
M_m	Material design variable	$a \otimes b$	Vector outer product
N	Database size	$MSE()$	Mean squared error
N_p	Number of reinforcement particles in a RVE	$P()$	Probability of ()
\hat{p}	Predicted quantity p	R^2	Correlation of determination
\bar{p}	Mean of target p	$Tr(A)$	The standard trace operator of a square matrix A
p^T	Transpose of a vector p	var	Variance
P	First Piola-Kirchhoff stress tensor		

References

- Beecroft, M., Digital interlooping: 3D printing of weft-knitted textile-based tubular structures using selective laser sintering of nylon powder, *Int. J. Fash. Des. Technol. Educ.*, 12(2), 2019, 218-224.
- Dinh, T. D., Weeger, O., Kaijima, S., Yeung, S.-K., Prediction of mechanical properties of knitted fabrics under tensile and shear loading: Mesoscale analysis using representative unit cells and its validation, *Compos. Part B Eng.*, 148, 2018, 81-92.
- Weeger, O. et al., Nonlinear Multi-Scale Modelling, Simulation and Validation of 3D Knitted Textiles, *Appl. Compos. Mater.*, 1-14.
- Yvonnet, J., Monteiro, E., He, Q.-C., Computational homogenization method and reduced database model for hyperelastic heterogeneous structures, *Int. J. Multiscale Comput. Eng.*, 11(3), 2013, 201-225.
- Le, B. A., Yvonnet, J., He, Q.-C., Computational homogenization of nonlinear elastic materials using neural networks, *Int. J. Numer. Methods Eng.*, 104(12), 2015, 1061-1084.
- Kaldor, J. M., James, D. L., Marschner, S., Kaldor, J. M., James, D. L., Marschner, S., Simulating knitted cloth at the yarn level, *ACM SIGGRAPH 2008 papers on - SIGGRAPH '08*, 27(3), 2018.
- Nadler, B., Papadopoulos, P., Steigmann, D. J., Multiscale constitutive modeling and numerical simulation of fabric material, *Int. J. Solids Struct.*, 43(2), 2006, 206-221.
- Jones, R. M., *Mechanics Of Composite Materials*, Taylor & Francis, 1998.
- Yeoman, M. S., Reddy, D., Bowles, H. C., Bezuidenhout, D., Zilla, P., Franz, T., A constitutive model for the warp-weft coupled non-linear behavior of knitted biomedical textiles, *Biomaterials*, 31(32), 2010, 8484-8493.
- Bessa, M. A. et al., A framework for data-driven analysis of materials under uncertainty: Countering the curse of dimensionality, *Comput. Methods Appl. Mech. Eng.*, 320, 2017, 633-667.
- Bessa, M. A., *Data-driven Multi-scale Analyses of Materials and Structures*, Ph. D. Thesis, Northwestern University, 2016.
- Geers, M. G. D., Kouznetsova, V. G., Matouš, K., Yvonnet, J., Homogenization Methods and Multiscale Modeling: Nonlinear Problems, *Encyclopedia of Computational Mechanics*, 2017, 1-34.
- Geers, M. G. D., Kouznetsova, V. G., Brekelmans, W. A. M., Multi-scale computational homogenization: Trends and challenges, *J. Comput. Appl. Math.*, 234(7), 2010, 2175-2182.
- Matouš, K., Geers, M. G. D., Kouznetsova, V. G., Gillman, A., A review of predictive nonlinear theories for multiscale modeling of heterogeneous materials, *J. Comput. Phys.*, 330, 2017, 192-220.
- Geers, M. G. D., Kouznetsova, V. G., Brekelmans, W. A. M., *Computational homogenization*, Springer, Vienna, 2010.
- Talebi, H., Silani, M., Bordas, S. P. A., Kerfriden, P., Rabczuk, T., A computational library for multiscale modeling of material failure, *Comput. Mech.*, 53(5), 2014, 1047-1071.
- Budarapu, P. R., Gracie, R., Yang, S. W., Zhuang, X., Rabczuk, T., Efficient coarse graining in multiscale modeling of fracture, *Theor. Appl. Fract. Mech.*, 69, 2014, 126-143.
- Fu, A., Chu-Chun, Torre, J. D., Willaime, F., Bocquet, J. L., Barbu, Multiscale modelling of defect kinetics in irradiated iron, *Nat. Mater.*, 4, 2005, 68-74.
- Bruix, K. A., Margraf, J. T., Andersen, M., Reuter, First-principles-based multiscale modelling of heterogeneous catalysis, *Nat. Catal.*, 2, 2019, 659-670.
- Rubia, M. J., Diaz, T., Khraishi, T. A., Wirth, B. D., Victoria, M., Caturla, Multiscale modelling of plastic flow localization in irradiated materials, *Nature*, 406, 2000, 871-874.
- Yip, M. P. S., Short, Multiscale materials modelling at the mesoscale, *Nat. Mater.*, 12, 2013, 774-777.
- Rabczuk, T., Gracie, R., Song, J., Belytschko, T., Immersed particle method for fluid – structure interaction, *Int. J. Numer. Meth. Engng.*, 2010, 48-71.
- Mitchell, T. M., *Machine Learning*, McGraw-Hill, Inc. New York, 1997.
- Bishop, C. M., *Pattern recognition and machine learning*, Springer, 2006.
- Guo, H., Zhuang, X., Rabczuk, T., Guo, H., Zhuang, X., Rabczuk, T., A Deep Collocation Method for the Bending Analysis of Kirchhoff Plate, *Comput. Mater. Contin.*, 58(2), 2019, 433-456.
- Anitescu, C., Atroshchenko, E., Alajlan, N., Rabczuk, T., Anitescu, C., Atroshchenko, E., Alajlan, N., Rabczuk, T., Artificial Neural Network Methods for the Solution of Second Order Boundary Value Problems, *Comput. Mater. Contin.*, 59(1), 2019, 345-359.
- Samaniego, E. et al., An energy approach to the solution of partial differential equations in computational mechanics via machine learning: Concepts, implementation and applications, *Comput. Methods Appl. Mech. Eng.*, 362, 2020, 112790.
- Rasmussen, C. E. and Williams, C. K. I., *Gaussian processes for machine learning*, MIT Press, 2006.
- Pedregosa, F. et al., Scikit-learn: Machine Learning in {Python}, *J. Mach. Learn. Res.*, 12, 2011, 2825-2830.
- Goodfellow, I., Bengio, Y., Courville, A., *Deep Learning*, MIT Press, 2016.
- McHutchon, A., *Differentiating Gaussian Processes*, 2013.
- Rogers, S. and Girolami, M., *A First Course in Machine Learning*, Taylor & Francis, 2011.
- Vassiliadis, S. G., Kallivretaki, A. E., Provatidis, C. G., Mechanical simulation of the plain weft knitted fabrics, *Int. J. Cloth. Sci. Technol.*, 19(2), 2007, 109-130.
- Vassiliadis, S., Kallivretaki, A., Provatidis, C., Geometrical modelling of plain weft knitted fabrics, *Indian J. Fibre Text. Res.*, 32, 2007, 62-71.
- Liu, Z., Bessa, M. A., Liu, W. K., Self-consistent clustering analysis: An efficient multi-scale scheme for inelastic heterogeneous materials, *Comput. Methods Appl. Mech. Eng.*, 306, 2016, 319-341.

ORCID iD

Sumudu Herath  <https://orcid.org/0000-0002-4462-4902>

Udith Haputhanthri  <https://orcid.org/0000-0003-1609-3822>



© 2021 Shahid Chamran University of Ahvaz, Ahvaz, Iran. This article is an open access article distributed under the terms and conditions of the Creative Commons Attribution-NonCommercial 4.0 International (CC BY-NC 4.0 license) (<http://creativecommons.org/licenses/by-nc/4.0/>).



How to cite this article: Herath, S., Haputhanthri U. Nonlinear Material Modelling and Design using Statistical Learning, *J. Appl. Comput. Mech.*, 7(3), 2021, 1583–1592. <https://doi.org/10.22055/JACM.2021.36106.2795>

Publisher's Note Shahid Chamran University of Ahvaz remains neutral with regard to jurisdictional claims in published maps and institutional affiliations.

